

3D Reconstruction of Occluded Luminous Objects

Akira Nagatsu, Fumihiko Sakaue and Jun Sato
Nagoya Institute of Technology, Nagoya 466-8555, Japan

Keywords: NLOS, Occluded Objects, Luminous Object, 3D Reconstruction, GAN, Luminance Distribution.

Abstract: In this paper, we propose a method for recovering the 3D shape and luminance distribution of an invisible object such as a human around a corner. The human body is a heat-generating object, so it does not emit visible light but emits far-infrared light. When a luminous object is around the corner, it cannot be observed directly, but the light emitted by the luminous object reflects on the floor or wall and reaches the observer. Since the luminous intensity of an object such as a human body surface is not uniform and unknown, its 3D reconstruction is not easy. In this paper, we propose a method to recover an occluded luminous object with non-uniform luminance distribution from changes in intensity patterns on the intermediate observation surface.

1 INTRODUCTION

Measuring the shape, location, and speed of an unseen object such as a human around the corner is very important for avoiding accidents on the road. The recovery of information on occluded objects is called NLOS (Non-Line of Sight), and research in this field has advanced in recent years (Velten et al., 2012; Chen et al., 2019).

However, the conventional NLOS methods require special measurement systems that scan and irradiate the laser beam and also require prior measurement of the reflectance of the observation surface, such as a wall surface. Therefore, we in this paper propose a new method for the 3D reconstruction of occluded objects without using active light illumination and without knowing the reflectance of the observation surface.

Generally, in human recognition and reconstruction, the human body is treated as an object that does not emit light. However, since the human body is a heat-generating object, it emits far-infrared light. Therefore, in the far-infrared region, the human body can be considered a luminous object. In this paper, we propose a method for recovering the 3D structure of a luminous object such as a human body that exists in an invisible position by using indirect light.

As shown in Fig. 1, the light emitted by the luminous object reflects on the floor or wall and reaches the observer. Thus, the observer can observe the indirect light emitted by the luminous object. The luminous intensity of a luminous object is in general not uniform but varies from point to point. Thus,

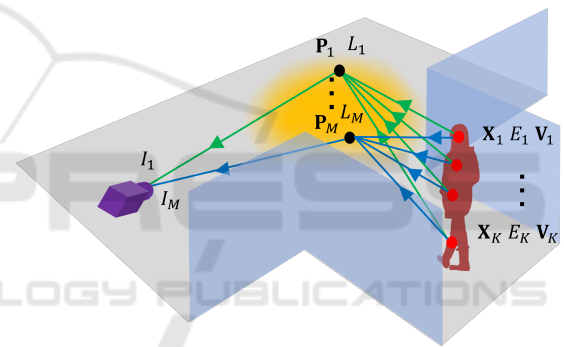


Figure 1: Indirect observation of luminous objects.

we aim to realize 3D reconstruction of occluded luminous objects with non-uniform luminance distribution. For this objective, we propose a method for recovering the luminance distribution E and 3D shape \mathbf{X} of the luminous object simultaneously from indirect light observation images I . In this paper, we assume that the camera is appropriately selected according to the wavelength of light emitted from the luminous object, and treat visible light and invisible light without distinction.

2 RELATED WORK

The recovery of information on objects in occluded locations is called NLOS (Non-Line of Sight) measurement, and its research has been progressing in recent years. In general, NLOS measurements are performed by projecting a laser beam or other light onto a wall and observing the reflected light coming back

from the object through the wall surface. (Velten et al., 2012; Chen et al., 2019). For this reason, these NLOS methods require complex optics and special observation systems that scan and measure the laser or beam light at high speed.

In contrast, in recent years, Some methods for recovering an occluded scene only from images passively observed by a camera have been developed. Most of these methods are based on placing some shielding objects between the scene and the wall, and using the half-shadow information produced by the shielding objects (Bouman et al., 2017; Saunders et al., 2019; Yedidia et al., 2019). However, these methods can only recover 2D image information of the scene, and cannot recover 3D shapes of objects in the scene. A method for recovering the light field in the scene has also been proposed. (Baradad et al., 2018). However, this method can only recover 2D images at multiple viewpoints and cannot recover 3D objects in the scene which are the source of the light field. In other words, this method cannot obtain the correspondence of light rays in the light field.

On the other hand, there are some attempts to perform 3D measurements by passive NLOS observation of luminous objects (Maeda et al., 2019; Kaga et al., 2019). However, these are limited to the estimation of a single light source or planar luminous objects with uniform luminous intensity. No generalized method for estimating the 3D shape of a luminous object and its non-uniform luminance distribution has been considered so far.

Thus, we in this paper propose a method for recovering 3D structure and non-uniform luminance distribution of occluded luminous objects. We believe that this is the first paper to tackle this difficult problem.

3 PROPOSED METHOD

3.1 Indirect Observation of Luminous Objects

Suppose a luminous 3D object and a camera that observes it are separated from each other by a wall and are positioned so that they cannot see each other as shown in Fig. 1. The light emitted from the luminous object is diffusely reflected at an intermediate observation surface such as a wall or floor, and the reflected light is observed by the camera.

In this paper, the 3D shape of a luminous object is represented by K 3D points $\mathbf{X}_k = [X_k, Y_k, Z_k]^\top$ ($k = 1, \dots, K$), and each of these 3D points has a different luminous intensity E_k ($k = 1, \dots, K$).

When the surface is illuminated by these K light source points \mathbf{X}_k , the illuminance L_m ($m = 1, \dots, M$) at M points \mathbf{P}_m ($m = 1, \dots, M$) on the observed surface can be described as follows:

$$L_m = \sum_{k=1}^K \frac{V_{km} E_k \cos \theta_{km}}{\|\mathbf{X}_k - \mathbf{P}_m\|^2} \quad (1)$$

where, θ_{km} represents the angle between the surface normal \mathbf{N}_m at point \mathbf{P}_m on the observation surface and the direction of the light source \mathbf{X}_k . Assuming that the observation surface is planar, θ_{km} can be described by using the surface normal \mathbf{N}_m as follows:

$$\cos \theta_{km} = \frac{(\mathbf{X}_k - \mathbf{P}_m) \cdot \mathbf{N}_m}{\|\mathbf{X}_k - \mathbf{P}_m\|} \quad (2)$$

V_{km} represents the visibility, and it takes 1 if the source point \mathbf{X}_k is visible from \mathbf{P}_m on the observation surface, and takes 0 if it is invisible.

Suppose the reflectance of the point \mathbf{P}_m on the observation surface is ρ_m , and the nonlinear intensity response function of the camera is C . Then, the intensity I_m of point \mathbf{P}_m observed by the camera can be described as follows:

$$I_m = C[\rho_m L_m] \quad (3)$$

In this paper, we assume that the response function C can be obtained a priori and consider the normalized intensity J_m , in which the effect of C is removed as follows:

$$J_m = C^{-1}[I_m] = \rho_m L_m \quad (4)$$

Unfortunately, it is not possible to obtain the 3D structure of the light source \mathbf{X}_k ($k = 1, \dots, K$) from the M intensity values J_m ($m = 1, \dots, M$) in the image. This is because there are a total of $M + 4K$ unknowns ($3K$ of the 3D point coordinates, K of their luminances, and M of the reflectance of the observed surface), while there are only M intensity information obtained by observation. Therefore, no matter how many observation points M are increased, the 3D points cannot be recovered. One way would be to measure the reflectance of the observed surface in advance, but this would severely hamper its application to unknown scenes. Thus, in the next section, we solve this problem by using observations at multiple time instants assuming that the luminous object is moving in the scene.

3.2 Recovering Occluded 3D Luminous Objects

Suppose a 3D luminous point \mathbf{X}_k is moving in the 3D space and its motion is $\mathbf{V}_k = [V_{Xk}, V_{Yk}, V_{Zk}]^\top$. The 3D

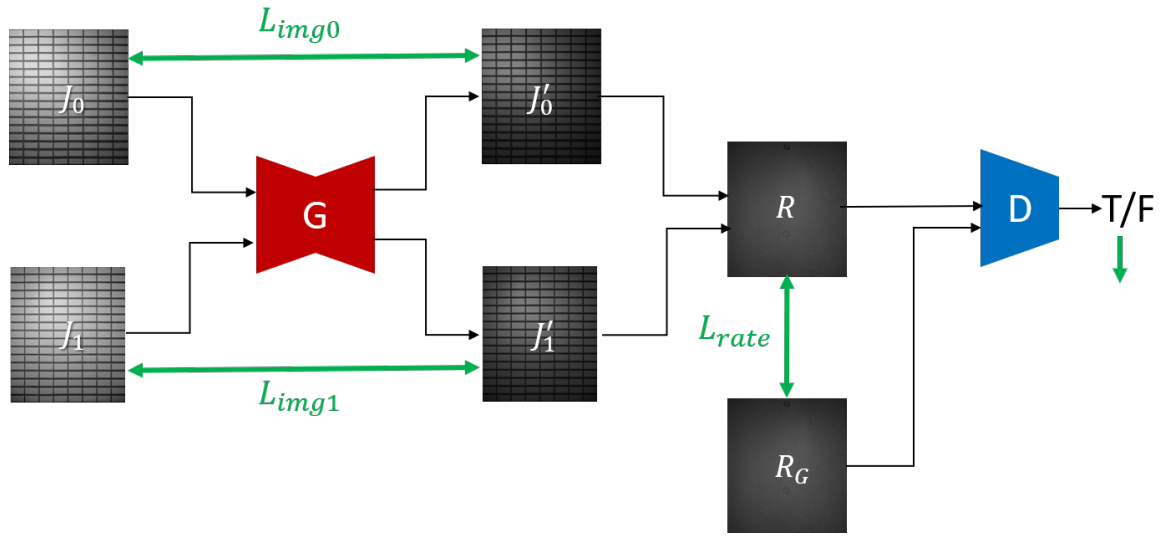


Figure 2: Network used in our method, which generates a pair of specular-free images from input camera images.

luminous object can be rigid or non-rigid, so the motion of the 3D luminous points can be different or the same from point to point. Then, the luminous point existing at \mathbf{X}_k at the current time exists at $\mathbf{X}_k - t\mathbf{V}_k$ at t time ago. Thus, the intensity J'_m observed at t time ago can be described as follows:

$$J'_m = \rho_m \sum_{k=1}^K \frac{V_{km} E_k \cos \theta_{km}^t}{\|\mathbf{X}_k - t\mathbf{X}_k - \mathbf{P}_m\|^2} \quad (5)$$

where, $\cos \theta_{km}^t$ is the angle between the direction of the light source and the surface normal at time t , and can be expressed as follows:

$$\cos \theta_{km}^t = \frac{(\mathbf{X}_k - t\mathbf{X}_k - \mathbf{P}_m) \cdot \mathbf{N}}{\|\mathbf{X}_k - t\mathbf{X}_k - \mathbf{P}_m\|} \quad (6)$$

Now, since the reflectance ρ_m of point \mathbf{P}_m is invariant before and after the light source motion, the ratio R of the intensity J'_m at the current time to the intensity J'_m at time t is invariant to the reflectance ρ_m , as in the following equation:

$$\begin{aligned} R'_m &= \frac{J'_m}{J'_m} \\ &= \frac{\sum_{k=1}^K V_{km} E_k \cos \theta_{km}^t \|\mathbf{X}_k - t\mathbf{X}_k - \mathbf{P}_m\|^{-2}}{\sum_{k=1}^K V_{km} E_k \cos \theta_{km}^0 \|\mathbf{X}_k - \mathbf{P}_m\|^{-2}} \quad (7) \end{aligned}$$

In this paper, we use R'_m obtained in this way and perform a 3D reconstruction of the light sources without knowing the reflectance of each surface point. As a result, our method can recover the 3D structure of the light source object, even if the reflectance of the intermediate observation surface is not uniform and unknown.

The 3D reconstruction of the light source is performed by simultaneously determining the light

source position \mathbf{X}_k , the light source intensity E_k and velocity \mathbf{V}_k ($k = 1, \dots, K$), which minimize the error between the observed intensity obtained by the camera and the observed intensity computed from Eq. (7) as follows:

$$\begin{aligned} &\{\mathbf{X}_1, E_1, \mathbf{V}_1, \dots, \mathbf{X}_K, E_K, \mathbf{V}_K\} \\ &= \arg \min \sum_{t=1}^{T-1} \sum_{m=1}^M \|R'_m - \hat{R}'_m\| \quad (8) \end{aligned}$$

In this research, we used matlab optimization function for this estimation.

However, this estimation has an ambiguity with respect to the magnitude of light source luminance. Therefore, we fix the luminance of one of the light sources to 1 and compute the relative luminance of the remaining light sources. In our experiments, the estimation was performed with $E_1 = 1$.

Now, let us now consider the conditions under which the proposed method works. The proposed method obtains $M(T-1)$ observations R by observing the intensity at T times ($T \geq 2$) at M points on the observation surface. On the other hand, the unknowns to be obtained are K 3D coordinates of each light source point, K light source intensity, and K 3D motions. Since we have an indefiniteness of magnitude with respect to light source intensity, the number of unknowns to be computed is $7K - 1$.

Therefore, under the condition that the following inequality holds, the positions, luminous intensities, and motions of all light source points can be obtained from the observed image intensity:

$$M(T-1) \geq 7K - 1 \quad (9)$$

In our experiments, we show that 3D reconstruction is possible under these conditions.

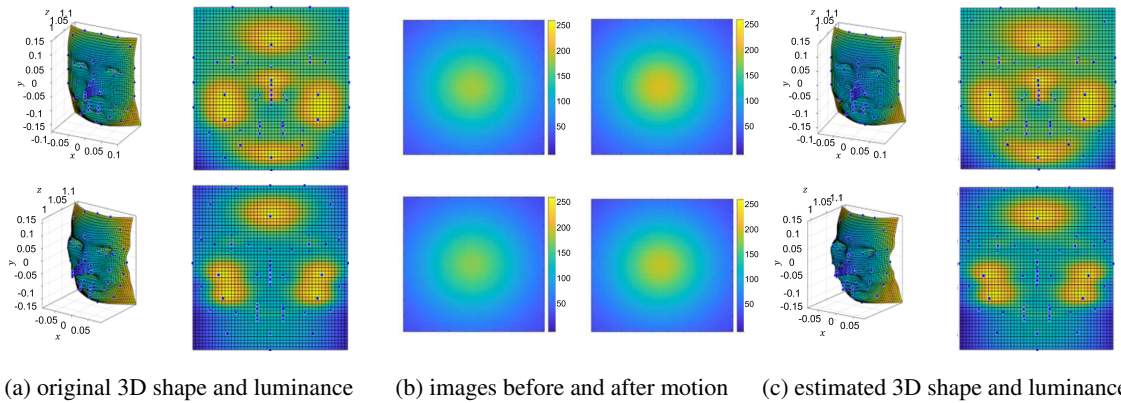


Figure 3: 3D luminous objects used in synthetic image experiments, observed images, and recovered results.

4 REMOVAL OF SPECULAR REFLECTION

Up to now, we have considered the case where an intermediate observation surface such as a wall has an ideal diffuse reflection. However, real intermediate surfaces such as walls and floors also have specular reflections in general. Therefore, we next describe a method for generating an ideal input image by removing specular reflection components from the real input image. By using the ideal input image obtained in this way, the proposed method described in section 3 works properly.

In this paper, we remove the specular reflection components in real images by using conditional GAN (Mirza and Osindero, 2014), (Isola et al., 2017), which is trained to generate specular reflection-free images from input camera images.

As described in section 3, we in this research perform 3D reconstruction using the ratio of the intensity of two images, J_0 and J_1 , obtained before and after moving the light source. Thus, we train our network so that the network takes a pair of images $\{J_0, J_1\}$ as input and output a pair of specular-free images $\{J'_0, J'_1\}$. The network is trained so that the ratio R of the generated images, J'_0 and J'_1 , becomes the ground truth ratio R_G . The ground truth ratio can be obtained by using Eq. (7).

Fig. 2 shows our network for generating a pair of specular-free images. Generator (G) generates a pair of images $\{J'_0, J'_1\}$ by removing the specular reflection component from a pair of camera images $\{J_0, J_1\}$. Then, we generate an image R by taking the pixel-wise ratio of J'_0 and J'_1 , and compare it with its ground truth image R_G for computing the loss L_{rate} . Also, the discriminator (D) is used for adversarial learning, and it learns to discriminate between R and R_G by using

the adversarial loss L_{GAN} .

The training is performed by minimizing the following loss for various light source configurations, light source motions, light source intensities, and reflectance of intermediate surfaces:

$$L = L_{rate} + \lambda_1(L_{img0} + L_{img1}) + \lambda_2 L_{smooth} + \lambda_3 L_{GAN} \quad (10)$$

where, L_{img0} and L_{img1} is the difference between the input and output images at the two time instants, and L_{smooth} is the smoothness of R .

5 EXPERIMENT

5.1 Synthetic Image Experiment

We next show the experimental results from our method. We first tested our method by using synthetic images. In this experiment, we used synthetic human faces as luminous objects, and their 3D shape and non-uniform luminance distributions were recovered by using the proposed method. Fig. 3 (a) shows the 3D shape and non-uniform luminance distribution of two different faces. The size of the face is approximately 30 cm x 20 cm in length and width.

These luminous objects were placed 100 cm away from the wall surface and approached the wall at a speed of 5 cm/frame. The images observed on the wall before and after the object motion are shown in Fig. 3 (b). These images show that the observed intensity increases as the object gets closer to the wall surface. We used these images for recovering the 3D shape and luminance distribution of faces by using our method.

The size of the image is 45×45 , so the number of observations M is 2025. The number of luminous

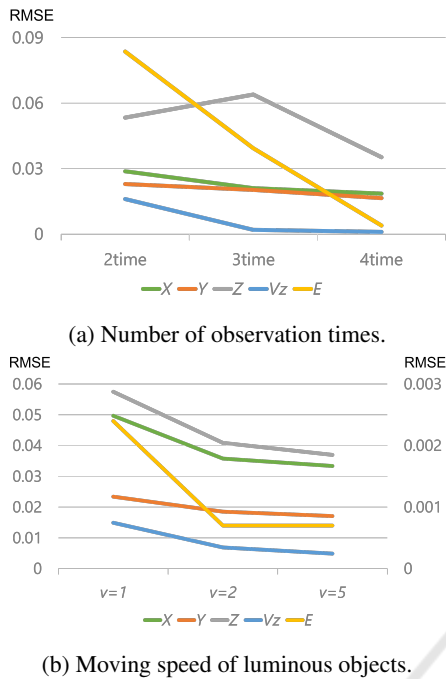


Figure 4: Relationship between the number of observation times, the moving speed of luminous objects, and the accuracy of estimation (RMSE).

points is 57 for face1 and 55 for face 2, so the information to be recovered is 57×7 for face1 and 55×7 for face2. Thus, we have a sufficient number of observations for 3D reconstruction.

The 3D shapes and luminance distributions recovered by using the proposed method are shown in Fig. 3 (c). Comparing (a) with (c), we find that both the 3D shape and the luminance distribution can be estimated quite accurately. These results show that the 3D shape of an occluded object and its luminance distribution can be recovered from indirect image observation through a wall by using the proposed method.

5.2 Quantitative Evaluation

We next present the results of a quantitative evaluation of the proposed method using synthetic images.

In the proposed method, reconstruction can be performed with observations at a minimum of two time instants, but it can be expected that the more time images are used, the more information will be obtained and the better estimation will be made. Therefore, we evaluated the estimation accuracy while increasing the number of times used from 2 to 4.

Fig. 4 (a) shows the change in accuracy (RMSE) of estimated shape (X, Y, Z), luminous intensity E , and velocity V_z . As can be seen from this figure, in-

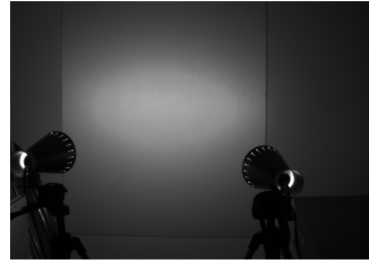


Figure 5: Experimental setup. Two light sources were used, and the intensity of the wall illuminated by these light sources was observed with a camera.

creasing the number of observation times significantly improves the accuracy of estimation of both shape, luminous intensity, and velocity.

We next evaluate the change in accuracy due to differences in the motion speed of the luminous object. Fig. 4 (b) shows the estimation accuracy (RMSE) when the moving speed is 5cm, 10cm, and 25cm per frame. The left scale of the graph represents position (X, Y, Z) and velocity V_z errors, while the right scale represents light source luminance E errors. From this graph, we find that the estimation accuracy is also highly dependent on the speed at which the object is moving.

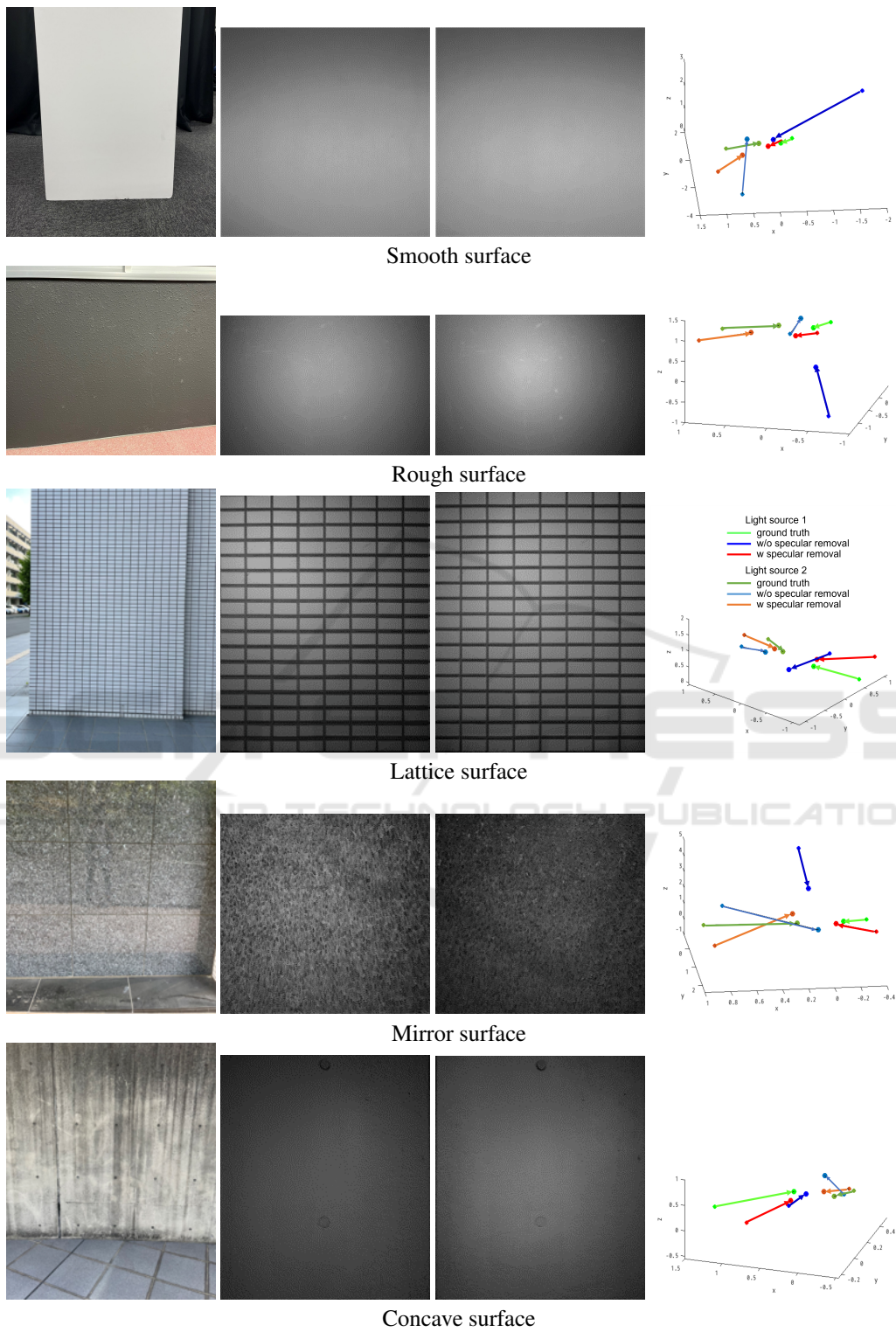
5.3 Real Image Experiments

We next show reconstruction results from real images. In this experiment, a visible light camera was used to perform a 3D reconstruction of an object emitting visible light.

Fig. 5 shows the experimental setup used in this experiment. As shown in the figure, two light sources were used, and the intensity of the wall illuminated by these light sources was observed with a camera to reconstruct the light source position, luminance intensity, and light source motion. Since the luminance of these light sources can be varied, the luminance of the two light sources were set to different values.

These light sources were moved at arbitrary speeds, and images were taken at two time instants before and after the motion. To eliminate the influence of ambient light, we also acquired an image with the light source off and subtracted from the image with the light source on to obtain an image illuminated only by the light source.

Since our method is invariant to the reflectance of the intermediate observation surface and is not affected by the texture on the surface, we tested our method using five different walls as intermediate observation surfaces. Fig. 6 (a) shows five different walls used in this experiment, which are



(a) observation surface (b) image before motion (c) image after motion (d) estimated motion

Figure 6: Observation surfaces, observed images, and recovered light source motions in real image experiment. Points and arrows in (d) show the position and motion of light sources.

Table 1: Comparison of restoration accuracy (RMSE) by removal of specular reflection component

	before removal (m)	after removal (m)
Smooth surface	4.759	1.555
Rough surface	8.068	1.716
Lattice surface	9.325	2.474
Mirror surface	7.633	1.853
Concave surface	7.412	1.989

smooth surface, rough surface, lattice surface, surface with strong specular reflection component (mirror surface), and concave surface. For removing the specular components by using the method shown in section 4, network training was performed with 720 training data and 180 test data.

Fig. 6 (b) and (c) show the observed images before the specular component removal, and Fig. 6 (d) shows the estimated results of the 3D light source positions before and after light source motion. The points and arrows show the position and motion of the light sources. Light and dark colors represent the first and second light sources respectively. The green arrows represent the ground truth light source motions, the blue arrows represent the light source motions recovered from the images before the specular component removal, and the red arrows represent the light source motions recovered from the images after the specular component removal. As shown in this figure, the proposed method can recover the occluded light source positions and motions from the indirect intensity on many different types of walls. This is because the proposed method uses the reflectance invariant for estimating the occluded light sources. In particular, the red arrows are closer to the green arrows, so we find that the specular component removal is effective in our method.

Table 1 compares the RMSE of the results recovered from the images before and after the specular component removal for each intermediate observation surface. From this table, we find that the accuracy of the estimation is drastically improved by removing the specular components using the method shown in section 4.

6 CONCLUSIONS

In this paper, we proposed a method for recovering the 3D structure and luminance distribution of luminous objects that cannot be directly observed from the camera. For this objective, we modeled the observation process of the light emitted from a luminous object, reflecting off walls and floors and reaching the

camera. Then, we showed that 3D shape and luminance distribution can be estimated simultaneously by using images obtained at multiple time instants. Experiments with synthetic and real images confirmed that the proposed method works under many different types of intermediate walls.

REFERENCES

- Baradad, M., Ye, V., Yedidia, A. B., Durand, F., Freeman, W. T., Wornell, G. W., and Torralba, A. (2018). Inferring light fields from shadows. In *Proceedings of the IEEE Conference on Computer Vision and Pattern Recognition*, pages 6267–6275.
- Bouman, K. L., Ye, V., Yedidia, A. B., Durand, F., Wornell, G. W., Torralba, A., and Freeman, W. T. (2017). Turning corners into cameras: Principles and methods. In *Proceedings of the IEEE International Conference on Computer Vision*, pages 2270–2278.
- Chen, W., Daneau, S., Mannan, F., and Heide, F. (2019). Steady-state non-line-of-sight imaging. In *Proceedings of the IEEE/CVF Conference on Computer Vision and Pattern Recognition*, pages 6790–6799.
- Isola, P., Zhu, J.-Y., Zhou, T., and Efros, A. A. (2017). Image-to-image translation with conditional adversarial networks. In *Proceedings of the IEEE conference on computer vision and pattern recognition*, pages 1125–1134.
- Kaga, M., Kushida, T., Takatani, T., Tanaka, K., Funatomi, T., and Mukaigawa, Y. (2019). Thermal non-line-of-sight imaging from specular and diffuse reflections. *IPSI Transactions on Computer Vision and Applications*, 11(1):1–6.
- Maeda, T., Wang, Y., Raskar, R., and Kadambi, A. (2019). Thermal non-line-of-sight imaging. In *2019 IEEE International Conference on Computational Photography (ICCP)*, pages 1–11. IEEE.
- Mirza, M. and Osindero, S. (2014). Conditional generative adversarial nets. *arXiv preprint arXiv:1411.1784*.
- Saunders, C., Murray-Bruce, J., and Goyal, V. K. (2019). Computational periscopy with an ordinary digital camera. *Nature*, 565(7740):472–475.
- Velten, A., Willwacher, T., Gupta, O., Veeraraghavan, A., Bawendi, M. G., and Raskar, R. (2012). Recovering three-dimensional shape around a corner using ultra-fast time-of-flight imaging. *Nature communications*, 3(1):1–8.
- Yedidia, A. B., Baradad, M., Thrampoulidis, C., Freeman, W. T., and Wornell, G. W. (2019). Using unknown occluders to recover hidden scenes. In *Proceedings of the IEEE/CVF Conference on Computer Vision and Pattern Recognition*, pages 12231–12239.